Title: Biomolecular Release from Alginate-Modified Electrode Triggered by Chemical Inputs Processed Through a Biocatalytic Cascade - Integration of Biomolecular Computing and Actuation

Authors: Evgeny Katz; Andrey V Okhokhonin, PhD; Sergii Domanskyi; Yaroslav Filipov; Maria Gamella, PhD; Alisa N Kozitsina, PhD; Vladimir Privman, PhD

To be cited as: 10.1002/elan.201700810

Link to VoR: https://doi.org/10.1002/elan.201700810

Biomolecular Release from Alginate-Modified Electrode Triggered by Chemical Inputs Processed Through a Biocatalytic Cascade – Integration of Biomolecular Computing and Actuation

Andrey V. Okhokhonin,[a, c] Sergii Domanskyi,[b] Yaroslav Filipov,[a, b] Maria Gamella,[a] Alisa N. Kozitsina,[c] Vladimir Privman,[b]* Evgeny Katz[a]*

[a] *Dr. A. V. Okhokhonin, Y. Filipov, Dr. M. Gamella, Prof. E. Katz*
Department of Chemistry and Biomolecular Science, Clarkson University, Potsdam, NY 13699 (USA)
E-mail: ekatz@clarkson.edu; Homepage: http://www.clarkson.edu/~ekatz
[b] *Y. Filipov, S. Domanskyi, Prof. V. Privman*
Department of Physics, Clarkson University, Potsdam, NY 13699 (USA)
E-mail: privman@clarkson.edu; Homepage: http://www.clarkson.edu/Privman
[c] *Dr. A. V. Okhokhonin, Dr. A. N. Kozitsina*
Department of Analytical Chemistry, Institute of Chemical Engineering, Ural Federal University Yekaterinburg, 620002, Russian Federation

ORCID identification numbers for the authors of this article can be found under https://doi.org/.....

Keywords: modified electrode; biomolecular computing; enzyme logic; signal-controlled release; alginate; biocatalytic cascade

Abstract

Biocatalytic cascades involving more than one or two enzyme-catalyzed step are inefficient inside alginate hydrogel prepared on an electrode surface. The problem originates from slow diffusion of intermediate products through the hydrogel from one enzyme to another. However, enzyme activity can be improved by surface immobilization. We demonstrate that a complex cascade of four consecutive biocatalytic reactions can be designed, with the enzymes

immobilized in an LBL-assembled polymeric layer at the alginate-modified electrode surface. The product, hydrogen peroxide, then induces dissolution of iron-cross-linked alginate, which results in release process of entrapped biomolecular species, here fluorescently marked oligonucleotides, denoted F-DNA. The enzymatic cascade can be viewed as a bio-computing network of concatenated AND gates, activated by combinations of four chemical input signals, which trigger the release of F-DNA. The reactions, and diffusion/release processes were investigated by means of theoretical modeling. A bottleneck reaction step associated with one of the enzymes was observed. The developed system provides a model for biochemical actuation triggered by a biocomputing network of reactions.

1. Introduction

Signal-triggered release of (bio)molecular species has been extensively studied over decades in many different contexts, primarily for controlled drug release and other biomedical applications [1-4]. Release processes from various micro/nano-porous materials [5,6] and polymer matrices [7,8] have been demonstrated. Different signal-responsive materials, particularly those sensitive to pH and temperature variation [9,10], as well as application of external magnetic field [11,12] or electrical potentials at conducting interfaces [13-15] have been used to activate the release processes. Among many other materials, alginate hydrogels attracted special interest because of their possible use as matrices for entrapment and controlled release of biomolecular species, including drugs [16,17]. Alginate hydrogels cross-linked with Ca^{2+} cations can be only used for slow release processes [18,19]. Recently, another kind of alginate hydrogel, cross-linked with Fe^{3+}-cations has been investigated for signal-triggered release of entrapped species [20]. While our previous study [20] was performed using alginate beads, the present work addresses the signal-release process from a thin-film electrochemically deposited on an electrode surface. This process is based on a special property of such alginate, which is that only Fe^{3+} cations facilitate alginate cross-linking, whereas Fe^{2+} cations do not cross-link alginate.

Indeed, Fe^{2+} is a “soft” metal cation that tends to bind neutral ligands containing nitrogen and sulfur, whereas Fe^{3+} cation is a typical example of a “hard” metal cation that preferentially

binds oxygen in negatively charged ligands, such as carboxylate groups [21], particularly in the alginate molecules. Thus, alginate can be easily converted from its soluble state to hydrogel upon electrochemical oxidation of Fe^{2+} to Fe^{3+} cations resulting in the formation of a hydrogel film on an electrode surface [22]. As alginate hydrogel film grows on the electrode surface, it can entrap various biomolecular species. The reverse process of dissolution of the resulting alginate hydrogel is accompanied by release of the entrapped species and can be easily triggered by electrochemical reduction of Fe^{3+} cations to Fe^{2+}. Reductive dissolution of alginate hydrogel film can be achieved by applying an appropriate potential on the modified electrode, providing an approach to electrochemically triggered biomolecular release [22], including drug release [23].

More sophisticated systems have been designed for inducing alginate dissolution and triggering the release process by application of biomolecular signals [24-32]. In these systems, the second electrode, which was equipped with biosensing elements generated the reductive potential/current which was then applied on the alginate-modified electrode, eventually resulting in alginate dissolution and biomolecular release. An advantage of this approach has been that, a wide variety of (bio)chemical signals and their combinations can be used for initiating the release process. A disadvantage, however, has been the complexity of the electrochemical systems requiring a combination of the biosensing and releasing electrodes.

The next step in advancing of the alginate release systems has been based on the known phenomenon of decomposition of the iron-cross-linked alginate in the presence of H_2O_2 [33-38]. This process involves a Fenton-type reaction catalyzed by iron cations and resulting in H_2O_2 breaking up into free radicals that are ultimately responsible for chopping up the alginate polymer, thus decomposing/dissolving the alginate film and releasing the entrapped species [39]. It has been recently demonstrated that this dissolution and the resulting release processes can be triggered by enzyme-catalyzed reactions producing H_2O_2, triggered by various combinations of chemical inputs, and taking place inside the hydrogel matrix. The reactions used, mimicked OR, AND, INHIB Boolean logic gates that utilize chemical "input signals" and produce H_2O_2 as the "output signal," controlling the release process from alginate [40]. A notable limitation of this approach has been that, the complexity of the biocatalytic reactions taking place in alginate hydrogel is limited by diffusion of intermediate products from one enzyme to another. Cascades

up to only two consecutive biocatalytic steps were realized [40], thus limiting the versatility of such signal-triggered systems.

In the present work we demonstrate that a *multistep biocatalytic cascade* can be successfully realized for triggering alginate hydrogel dissolution at the electrode surface and the accompanying release process, with the biocatalytic reactions taking place in a layer-by-layer (LBL)-assembled polymeric (polyelectrolyte) layer *at the interface* of the alginate film with the surrounding solution, rather than inside the hydrogel matrix. Here, we demonstrate that this approach allows to have four consecutive biocatalytic reactions in a cascade activated by combinations of four chemical-species input signals. The realized biocatalytic cascade can be viewed as a "biocomputing network" of concatenated Boolean logic gates in the framework of the recently developed unconventional computing [41] approach based on enzyme-catalyzed reactions [42,43]. The underlying mechanisms of this release process are then further investigated by means of theoretical modeling. Despite the fact that the cascade of four enzymatic reactions involves numerous chemical processes and diffusional transport of multiple species in hydrogel, at the interfacial region, and outside it, which could in principle require many parameters for precise modeling, our approach has allowed for quantitative characterization and experimental data fitting with relatively few key process parameters. Furthermore, modeling provides insight into the limiting reaction step. Overall, the biomolecular release from the alginate-modified electrode surface has been studied experimentally and modelled theoretically, allowing understanding the complex multi-step process performed at the electrode surface.

2. Materials and Methods

2.1. Materials

Amyloglucosidase (AMG; E.C. 3.2.1.3) from *Aspergillus niger*, glucose dehydrogenase (GDH; E.C. 1.1.1.47) from *Pseudomonas* sp., L-lactate dehydrogenase (LDH; E.C. 1.1.1.27) from bovine heart, lactate oxidase (LOx; E.C. 1.1.3.2) from *Pediococcus* sp., horseradish peroxidase (HRP; 1.11.1.7), sodium alginate from brown algae (medium viscosity, ≥2000 cP),

β-nicotinamide adenine dinucleotide (NAD^+), β-nicotinamide adenine dinucleotide reduced (NADH), maltose, pyruvic acid (Pyr), lactic acid (Lac), 2,2′-azino-*bis*(3-ethylbenzothiazoline-6-sulfonic acid) (ABTS), 4-(2-hydroxyethyl)-1-piperazineethanesulfonic acid (HEPES-buffer), 2-amino-2-(hydroxymethyl)propane-1,3-diol (Tris-buffer), (1-ethyl-3[3-(dimethylamino)propyl] carbodiimide (EDC), *N*-hydroxysuccimide (NHS), poly(ethyleneimine) (PEI, 50% w/v solution in H_2O, M_w ~750,000), polyacrylic acid (PAA) average M_v ~450,000, polyethylene glycol (PEG, 50% w/v solution in H_2O), 4-aminoantipirine (4AAP), *N*,*N*-dimethylaniline (DMA), dodecylbenzenesulfonic acid solution (DBS), flavin adenine dinucleotide (FAD), and other standard organic and inorganic materials and reactants were obtained from Sigma-Aldrich or J. T. Baker. Custom made DNA oligonucleotide labeled with FAM fluorescent dye (F-DNA) was purchased from Integrated DNA Technologies Inc. (San Diego, CA): 6-FAM-5'-TAG AGT AAC CTC ACA CGG AAT GTT TC-3' (6-FAM attached to the DNA released is a fluorescein derivative: see the FAM structure in Figure 1). All experiments were carried out in ultrapure water (18.2 MΩ·cm; Barnstead NANOpure Diamond).

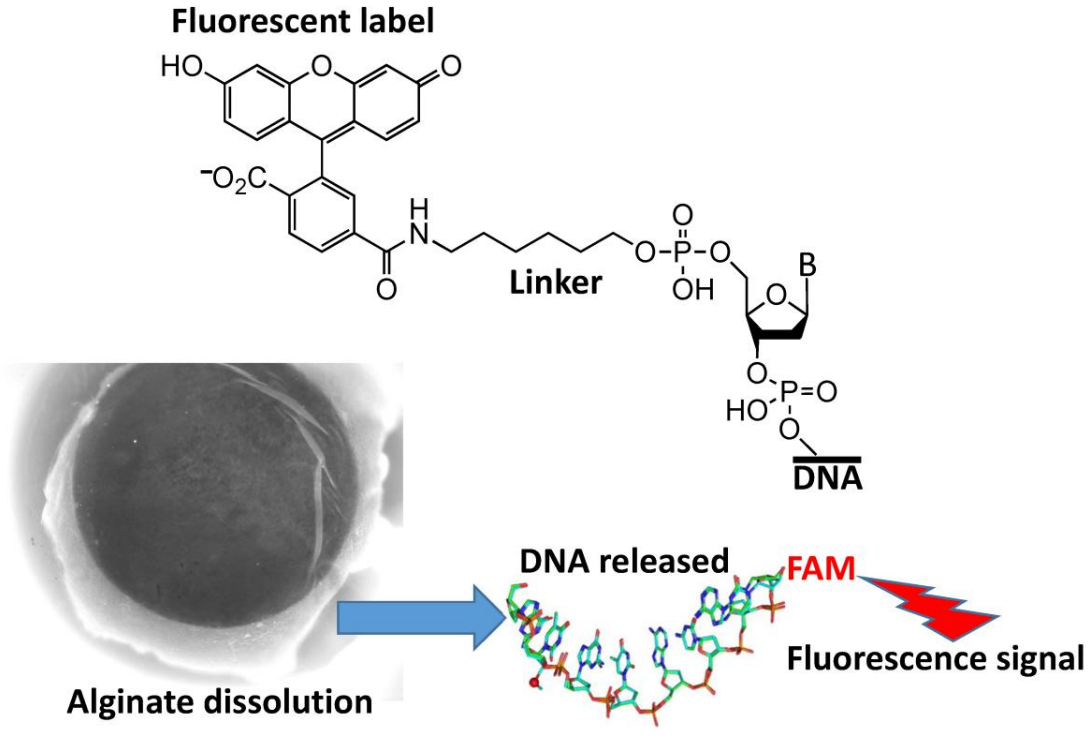

Figure 1. Schematic of the alginate decomposition process at the electrode surface, and (top) chemical structure of the FAM dye fluorescent label.

2.2. Instrumentation

Fluorescence measurements were performed using a fluorescent spectrophotometer (Varian, Cary Eclipse). A Shimadzu UV-2450 UV–Vis spectrophotometer was used for optical absorbance measurements. Electrochemical experiments were performed using an electrochemical workstation (ECO Chemie Autolab PASTAT 10) and GPES 4.9 (General Purpose Electrochemical System) software. All potentials were measured using a Metrohm Ag|AgCl|KCl, 3 M, reference electrode. Fluorescent images were obtained with Leica TCS SP5 II Tandem Scanning Confocal and Multiphoton Microscope.

2.3. Experimental Procedures

2.3.1. Preparation of the alginate-modified electrode

Before alginate deposition, graphite rods (ca. 1 mm diameter) were polished to mirror surface roughness with sandpaper (3M, 1000 grit) and then washed with ethanol and water 3 times in ultrasonic bath. Alginate (75 mg) was dissolved in 0.1 M Na_2SO_4 aqueous solution upon vigorous mixing on a magnetic stirrer at 45 ℃ overnight. Then 1 mL of this solution was mixed with 10 µL of 100 µM F-DNA and 120 µL of 0.3 M $FeSO_4$ aqueous solutions. Alginate deposition was performed by applying potential of 1.2 V to the working graphite electrode (working geometrical area immersed in the alginate solution 28 mm^2) for 180 s. After that, the alginate-modified electrode was rinsed with water, immersed in 1% w/v PEI solution for 180 s, rinsed with water again, and put in HEPES-buffer (25 mM, pH 7.4) for 2 hours resulting in deposition of PEI on the alginate film.

2.3.2. Enzyme immobilization in an LBL-assembled surface layer

The PEI-alginate-modified electrode was immersed in 100 µL of HEPES-buffer (25 mM, pH 7.4) containing 1% (w/w) PEG, 50 mM of EDC, 50 mM of NHS and 10 U of LOx for 2 hours. After that, the electrode was rinsed with the HEPES-buffer (25 mM, pH 7.4), and then

immersed successively in 1% (w/v) PAA solution in the HEPES-buffer for 180 s, in 1% (w/v) PEI solution in the HEPES-buffer for 180 s, and finally in 100 µL of the HEPES-buffer containing 1% (w/v) of PEG, 50 mM of EDC, 50 mM of NHS, 10 U of LDH, 10 U of GDH and 10 U of AMG for 2 hours. After immobilization, enzyme-functionalized alginate electrode was rinsed with HEPES-buffer, then with Tris-buffer (25 mM, pH 7.4), and left for 3 hours in Tris-buffer until uncontrolled leakage of F-DNA mostly stopped. Enzyme-functionalized alginate-modified electrode is abbreviated as EAE in what follows.

2.3.3. Analysis of the biocatalytic reaction cascade performed in solution

Hydrogen peroxide (H_2O_2) production during the cascade of enzymatic reactions taking place in solution was analyzed in order to verify no side reactions or "cross-talk" involving the various cascade processes would generate H_2O_2 bypassing the primary reaction pathway. This was done by following the increase absorbance at 415 nm, corresponding to the process of ABTS oxidation catalyzed by HRP. The reaction was performed in a Tris-buffer solution (50 mM, pH 7.4) containing ABTS (4 mM), horseradish peroxidase (1 U), LOx (10 U), LDH (10 U), GDH (10 U) and AMG (10 U). After 5 min of observation of the absorbance measure in the solution without any inputs, Pyr (5mM) was added to solution, then – NAD^+ (5 mM), after that – maltose (5 mM). Each successive addition was done once absorption leveled out at a constant value.

2.3.4. Analysis of the microscope images obtained from EAE

Microscope images were obtained with ×10-magnification of a front view of the electrode in passing light and by F-DNA fluorescence with excitation by blue light (488 nm).

2.3.5. F-DNA leakage/release measurement procedure

Signal inputs: *A*, *B*, *C*, and *D*, respectively, were defined as maltose (5 mM), NAD^+ (5 mM), pyruvic acid (Pyr; 5 mM), and molecular oxygen (O_2) dissolved in water in balance with air. The uncontrolled leakage and signal-triggered release of F-DNA were followed by measuring fluorescence at λ = 517 nm in a Tris-buffer solution (50 mM, pH 7.4). For these

measurements, EAE was placed in a cuvette (1 cm optical path) containing 1.5 mL Tris-buffer (50 mM pH 7.4). The uncontrolled leakage of F-DNA was measured without any additional component in the solution. The signal-controlled release process was triggered by adding maltose, NAD^+ and Pyr, considered as logic values **1**. The absence of these reactants (including the absence of O_2) was considered as logic value **0**. Removing molecular oxygen from the solution (when needed) was performed by bubbling with argon during the experiment. The solution was periodically mixed in order to provide a uniform distribution of the released F-DNA in it. The fluorescence intensity is linearly dependent on the F-DNA concentration. A calibration experiment, not detailed here, yielded the proportionality constant 1.12×10^{-3} nM (a.u.)$^{-1}$, necessary for the theoretical calculations reported in the next section.

3. Results and Discussion

In earlier approaches, one- and two-step biocatalytic reactions were realized in alginate films prepared electrochemically at an electrode surface [40]. These processes mimic Boolean logic gates and trigger biomolecular release. However, more complex biocatalytic cascades do not function effectively inside alginate hydrogel presumably because their successive steps involve diffusion-limited transport of intermediate products. In order to achieve a higher throughput multi-step biocatalytic reactions sequence, ultimately yielding H_2O_2 that diffuses into and decomposes the alginate hydrogel, which in turn releases entrapped biomolecular species, we assembled the biocatalytic system in an LBL-assembled polymeric film at the interface of the alginate film prepared at an electrode surface. It transpires that, enough of the intermediate-reaction products are retained in the vicinity of the hydrogel/water interface, reaching the next catalytic center much more effectively than inside the hydrogel.

The modified electrodes used in the present study were prepared by electrochemical deposition of the alginate hydrogel film cross-linked with Fe^{3+} cations. Four enzymes, AMG, GDH, LDH and LOx, have been covalently attached within the LBL layer at external surface of the hydrogel. The catalytic cascade, Figure 2A, included the following reactions: (*i*) each molecule of maltose was hydrolyzed to two molecules of glucose in the reaction catalyzed by AMG; (*ii*) then, glucose was oxidized and NAD^+ was reduced to yield NADH in the reaction

catalyzed by GDH; (*iii*) then, NADH reduced Pyr to Lac in the reaction catalyzed by LDH; and (*iv*) finally, Lac was oxidized by O_2 to yield H_2O_2 in the reaction catalyzed by LOx. The produced H_2O_2 can diffuse into the alginate hydrogel, which results in free radicals in a Fenton-type reaction catalyzed by iron cations. These free radicals then decompose the alginate hydrogel and release the entrapped biomolecular species. As a model for the latter, we included fluorescent-label functionalized oligonucleotides (denoted F-DNA, see the DNA sequence in Section 2.1) in the hydrogel. Its release was detected by measuring fluorescence in the solution. The 4-step biocatalytic cascade can yield H_2O_2 only if all the chemical input signals are applied to activate all the reaction steps. This mimics a network of concatenated AND gates, Figure 2B. Indeed, each reaction step (except the very first one) requires two reacting species: One produced *in situ* in the previous catalytic step and another added as the input signal, thus representing the AND Boolean gate. The very first step was activated by a single input (maltose), mimicking the Identity gate (ID).

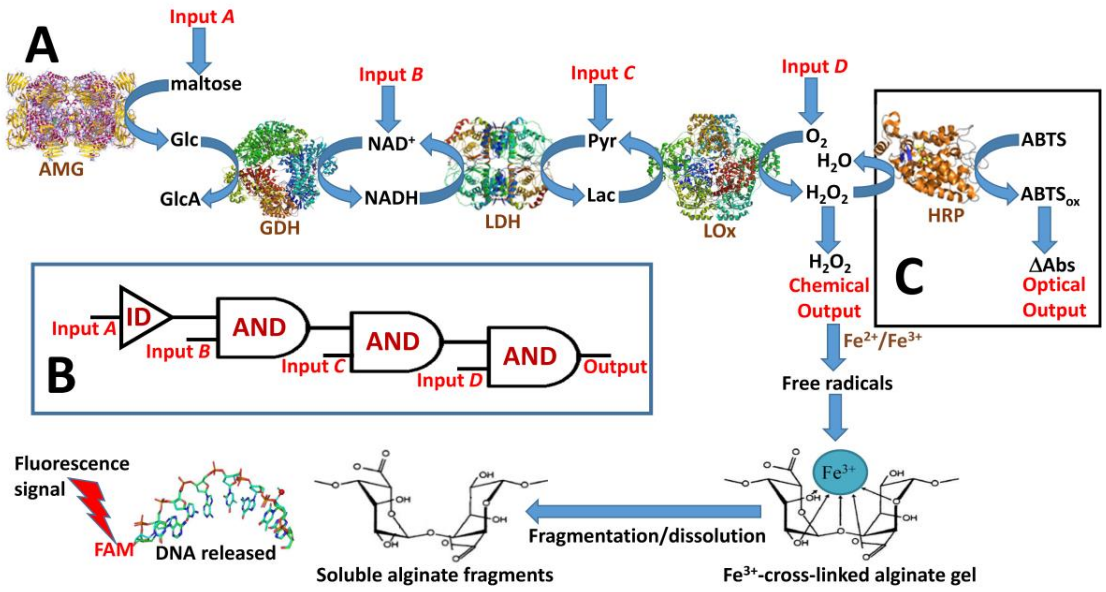

Figure 2. (A) The biocatalytic cascade shown schematically. The enzymes, AMG, GDH, LDH and LOx, were all immobilized at the electrode surface, and catalyzed reactions yielding H_2O_2 as the final product only when all the inputs (*A*, *B*, *C*, *D*) were applied at their logic values **1**. The produced H_2O_2 was catalytically decomposed by iron cations present in alginate, and the generated free radicals resulted in the degradation/fragmentation/dissolution of the film, allowing F-DNA release. (B) Logic

circuit composed of concatenated Identity (ID) and three AND gates corresponding to the biocatalytic cascade performed by the immobilized enzymes, shown in A. (C) The same biocatalytic cascade was also realized in a solution (using soluble enzymes), terminated by an additional reaction catalyzed by HRP and yielding ABTS oxidized ($ABTS_{ox}$), which was observed optically. All abbreviations are explained in the text; GlcA is gluconic acid (product of glucose oxidation).

Prior to studying the biocatalytic reactions of the enzymes immobilized at the surface of the alginate film, we performed the same reaction cascade with enzymes in solution; see Figure 2C. In this case the biocatalytically produced H_2O_2 was further reacted with HRP (one more enzyme used only in the experiment performed in solution) resulting in oxidation of ABTS to yield $ABTS_{ox}$, which causes an increase in absorbance at 415 nm. The reacting solution initially containing all 5 enzymes (AMG, GDH, LDH, LOx, HRP) ABTS and O_2, had additional input signal chemicals added sequentially in the following order: first Pyr, then NAD^+, and finally maltose. The optical absorbance at 415 nm was monitored during the experiment; see Figure 3. As expected, only the last addition step, that of maltose, resulted in the activation of the whole cascade. This rather straightforward experiment has confirmed that indeed there are no side reactions or "cross-talk" involving the various cascade processes that would generate H_2O_2 bypassing the primary reaction pathway.

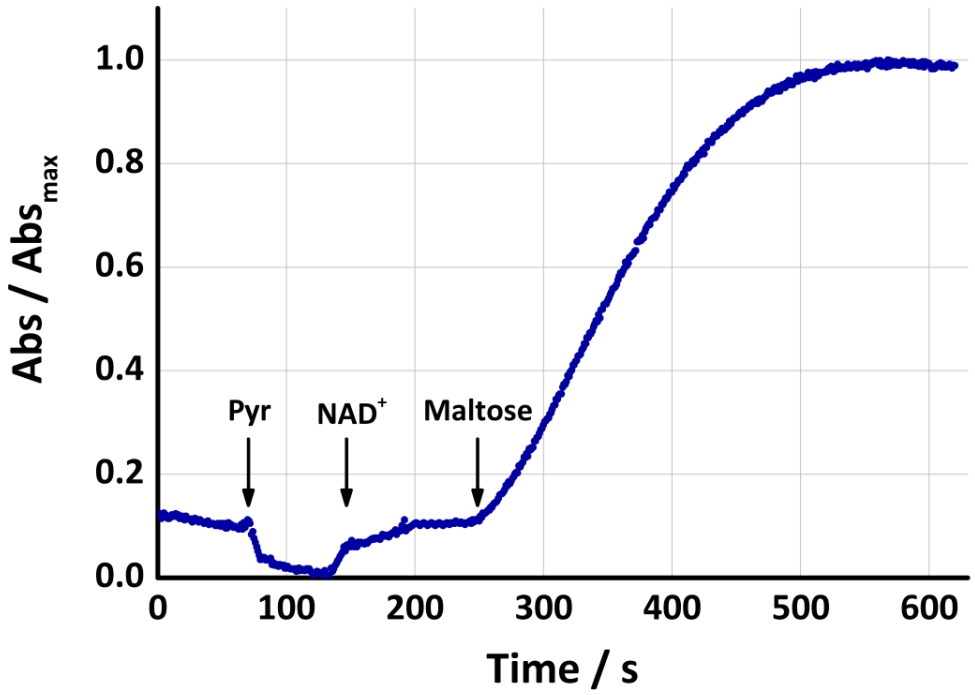

Figure 3. Optical absorbance changes (λ = 415 nm) generated by the cascade of reaction with enzymes AMG, GDH, LDH, LOx, and HRP in solution, catalyzing the formation of $ABTS_{ox}$ upon addition of all the initially absent inputs: Pyr, NAD^+, and maltose, in sequence; see Section 2.3.3 for the specific experimental conditions.

When similar reactions (excluding the HRP/ABTS process) were performed with immobilized enzymes, significant degradation/dissolution of the alginate hydrogel was achieved only when all the four input signals were applied; see Figure 4. It should be noted that the immobilized enzymes bound to the insoluble LBL polymer layer remain on the electrode surface while the alginate film is biocatalytically decomposed/dissolved, thus allowing almost complete disappearance of the alginate film, Figure 4.

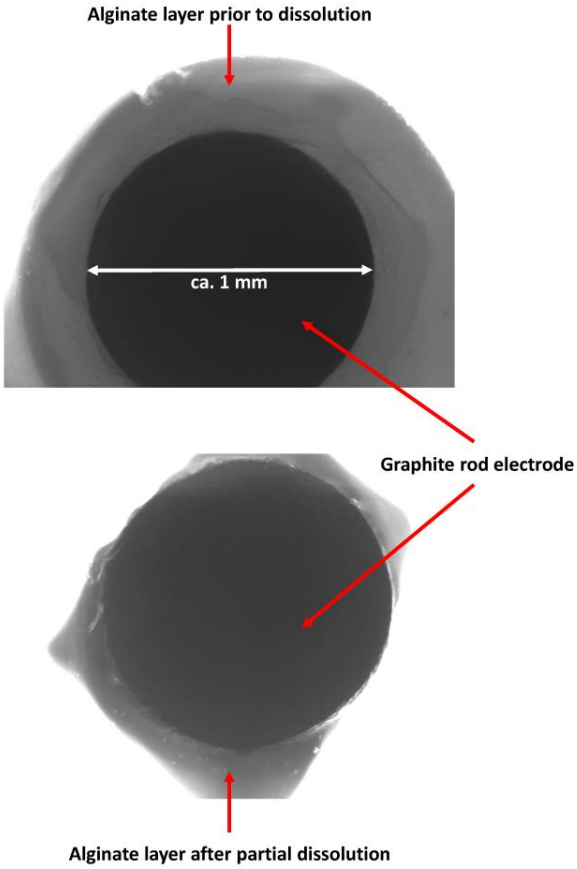

Figure 4. Microphotograph (×10 magnification, front view, ambient illumination) of typical EAE morphologies at the electrode surface. These electrodes were held in solution for 6 hours (top image) without application of inputs, and (bottom image) with all the inputs applied. The bottom image illustrates partial decomposition/dissolution of the alginate layer.

The enzymes immobilized at the surface of the alginate hydrogel film prepared electrochemically at the electrode surface can be activated stepwise, realizing systems with cascades reactions of different number of catalytic steps involved in the production of H_2O_2. In such experiments, we applied chemical species which would otherwise be produced *in situ*, had the whole catalytic cascade been active. When none of the inputs were applied, uncontrolled leakage of F-DNA from the alginate film was very limited, Figure 5(a). Applying the Lac input in the presence of O_2 results in activation of LOx, producing H_2O_2, dissolving alginate hydrogel and releasing F-DNA, Figure 5(b). Applying NADH and Pyr inputs instead (with O_2 present),

results in activation of the two-step process catalyzed by LDH and LOx, also producing H_2O_2, etc., Figure 5(c). Similarly, applying glucose, NAD^+ and Pyr (with O_2 present) results in activation of the three-step process catalyzed by GDH, LDH and LOx, Figure 5(d). Finally, applying maltose, NAD^+ and Pyr results in activation of the full four-step process catalyzed by AMG, GDH, LDH and LOx, Figure 5(e). When O_2 was not present, the LOx enzymatic step was not active, no H_2O_2 was formed or F-DNA released, and the measured data (not shown) overlapped with Figure 5(a).

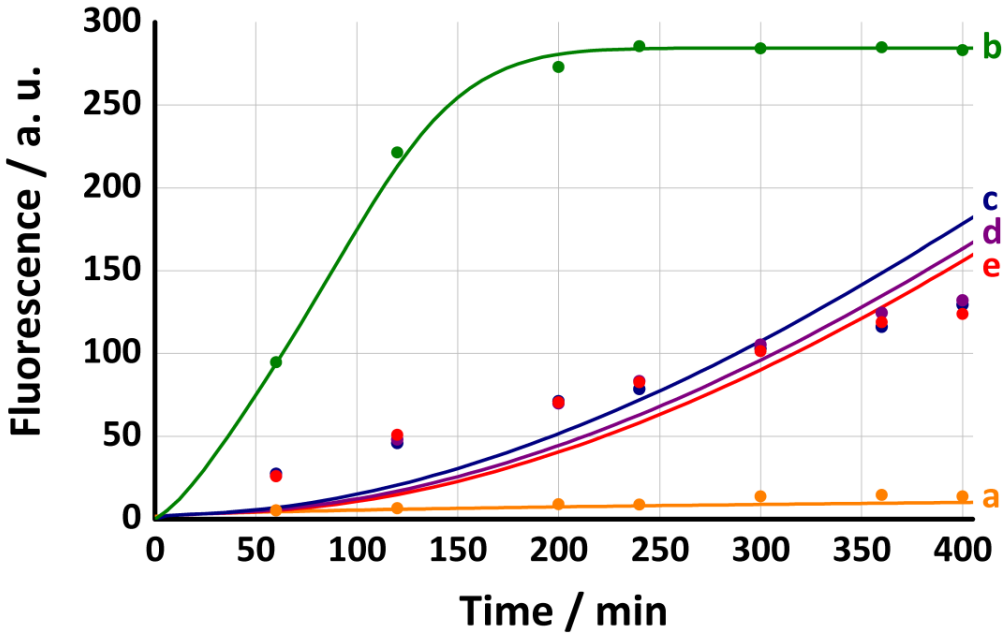

Figure 5. Fluorescence response at λ = 517 nm, with experimental data plotted as circles, with matching theoretical model curves, corresponding to the F-DNA leaked/released upon stepwise activation of the biocatalytic cascade: (a) leakage, (b) after addition of lactate (5 mM), (c) after addition of NADH (5 mM) and Pyr (5 mM), (d) after addition of Glc (5 mM), NAD^+ (5 mM) and Pyr (5 mM), (e) after addition of maltose (5 mM), NAD^+ (5 mM) and Pyr (5 mM).

Notably, the rate of the F-DNA release process was much higher when a one-step catalytic process activated by Lac was realized; see Figure 5. All the longer biocatalytic cascades that include more enzymes show practically the same, slower-induction time dependence. This

implies a rate-limiting process, which is likely due to the LDH-catalyzed step, as discussed later, when we report modeling results. Note that LDH is the second from the end enzyme of the catalytic cascade; see Figure 2A.

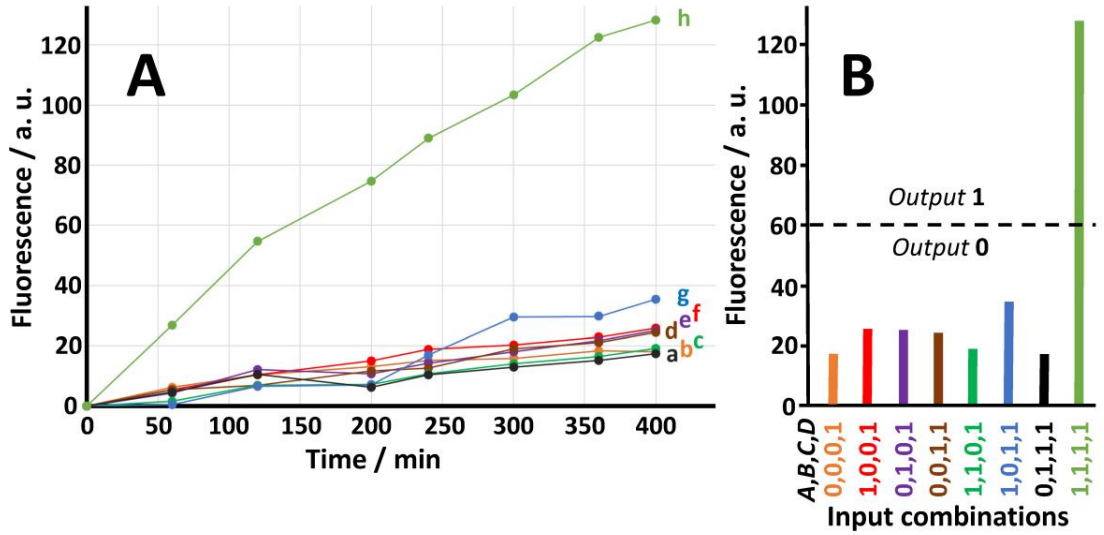

Figure 6. (A) Fluorescence response (λ = 517 nm) corresponding to the F-DNA released upon application of the input signals in several selected (out of total 16 possible) different combinations: (a) **0**,**1**,**1**,**1**; (b) **0**,**0**,**0**,**1**; (c) **1**,**1**,**0**,**1**; (d) **0**,**0**,**1**,**1**; (e) **0**,**1**,**0**,**1**; (f) **1**,**0**,**0**,**1**; (g) **1**,**0**,**1**,**1**; (h) **1**,**1**,**1**,**1**. The line segments were added to guide the eye. Note that the data set (h) here, is the same as in Figure 5(e). Only the **1**,**1**,**1**,**1** input combination yields F-DNA release, as expected for the concatenated binary gates. (B) The bar chart showing the fluorescence output corresponding to the released F-DNA, extracted from part A at 400 min reaction time. The "binary" digital distinction between **0** and **1** outputs is clearly well defined (as schematically marked by the broken line).

The enzymatic cascade can be viewed as carrying out a Boolean-logic network of gates; see Figure 2B. To illustrate this, we applied the input signals, *A*, *B*, *C*, *D* (maltose, NAD^+, Pyr, O_2, respectively) in several "binary-logic" combinations in attempt to activate the biocatalytic cascade and cause F-DNA release; see Figure 6. As expected for concatenated gates shown in Figure 2B, the final result **1** (significant F-DNA release) was observed only for the input signal combination **1**,**1**,**1**,**1**, while several other input combinations tested (means, some of the input

chemicals "added"/kept at zero concentrations) resulted in noticeably smaller fluorescence of the solution, which can be attributed to uncontrolled F-DNA leakage. It should be noted that the present "model system" realization of the enzyme-based logic system includes not only "binary" processing of the input signals, but also chemical actuation (alginate hydrogel degradation/dissolution and F-DNA release), offering a prototype not only for the "computing" signal processing, but also for the "machinery" actuation, for biomolecular release.

Our modelling approach considers the key steps in the cascade of enzymatic processes schematically shown in Figure 2A. Each enzyme functioning is a few- to multi-reaction process involving successive binding/reacting with that enzyme's substrate(s). However, an effective fewer-parameter approach suffices [44-46] for modeling the type of dynamics considered here. Indeed, we are considering the situation whereby each enzymatic process is "driven" by plentiful supplies of substrates (when they are present) in the LBL-polymeric layer at the surface and functioning in approximate steady-state with throughput that can be described in a single-rate-constant "effective" chemical reaction approximation [44-46]. These enzymatic processes take place at the interface of the alginate film on the graphite electrode. The latter is taken of radius $R = 0.45$ mm, the thickness of the film on its surface is $X = 0.2$ mm, the film covers length $Z = 10$ mm of the electrode. We also assume fast diffusion, with the diffusion coefficient $\mathcal{D}_0 = 7 \times 10^{-6}\text{cm}^2\ \text{s}^{-1}$, of all the mobile chemicals. For example, the input chemicals (and other chemicals added at time $t = 0$) are consumed inside thin layer near the polymer-solution interface, assumed of thickness 1 μm, and are replenished by diffusion from the bulk solution. The intermediate chemicals and final products, e.g. glucose, NADH, H_2O_2, diffuse into the polymer film and the bulk solution.

For the first step of the enzymatic cascade, we introduce the effective rate constant, k_1, for the conversion of maltose, $A(t)$, to glucose, $G(t)$, catalyzed by AMG:

$$A \overset{k_1}{\rightarrow} G\ . \qquad (1)$$

This rate constant lumps in it several process parameters, *including the enzyme's activity*. The introduced rate parameters, k_1 here, and those defined below, for convenience also include in

them the various stoichiometric factors. For example, a molecule of maltose actually yields two glucose molecules, unlike what is shown in the schematic Equation (1). The second input, NAD^+, denoted by $B(t)$, is required to oxidize glucose to gluconic acid by glucose dehydrogenase. The third input, pyruvate, $C(t)$, is reduced to lactate, $L(t)$, by lactate dehydrogenase. During the latter process NADH, $Q(t)$, is converted into its oxidized form. These processes are similarly approximated and involve two new effective rates:

$$G + B \overset{k_2}{\rightarrow} Q + \cdots , \tag{2}$$

$$Q + C \overset{k_3}{\rightarrow} B + L . \tag{3}$$

During the next step of the reaction cascade, lactate is oxidized by lactate oxidase back to pyruvate:

$$L + D \overset{k_4}{\rightarrow} C + H . \tag{4}$$

Note that oxygen, $D(t)$, is consumed in this process, which results in the final product, H_2O_2, $H(t)$. We assume that oxygen concentration in the bulk solution remains constant, $D(t) = 0.27$ mM (at 22 ℃) [47], for all times *t*, due to diffusion from the outside air. However, we did not lump it into the rate constant in Equation (4) in order to have the rate constants $k_{2,3,4}$ have the same units.

All the processes summarized above take place in the interfacial region (presumably, in a thin surface layer) of alginate, and due to unhindered diffusion, the reactants' concentrations equilibrate fast outside the bulk of alginate, including within the interfacial region. Moreover, the hydrogen peroxide establishes approximately constant concentration not only in the interfacial region but also deep enough within the bulk of the alginate to cause volumetrically significant degradation/ dissolution of the latter. These reactions are phenomenologically described by the following rate equations:

$$\frac{dA(t)}{dt} = -k_1 A(t)\ ,$$
$$\frac{dG(t)}{dt} = k_1 A(t) - k_2 G(t)B(t)\ ,$$
$$\frac{dB(t)}{dt} = -\frac{dQ(t)}{dt} = -k_2 G(t)B(t) + k_3 Q(t)C(t)\ , \qquad (5)$$
$$\frac{dC(t)}{dt} = -\frac{dL(t)}{dt} = -k_3 Q(t)C(t) + k_4 L(t)D(t)\ ,$$
$$\frac{dD(t)}{dt} = -\frac{dH(t)}{dt} = -k_4 L(t)D(t)\ .$$

Inside alginate, hydrogen peroxide causes reduction of cross-linking due to free radicals produced on the iron cations in Fenton-type reactions:

$$\frac{\partial H(r,t)}{\partial t} = \frac{\partial W(r,t)}{\partial t} = -k_5 H(r,t)W(r,t)\ . \qquad (6)$$

Here, we use the same expression and the same parameter values as in an earlier study [20] of a different alginate system. The crosslinking density is inversely proportional to the void sizes in alginate [48]. As this density, $W(r,t)$, which is initially $W_0 = 0.85$ mM, decreases, the diffusion coefficient of the entrapped F-DNA increases. Here we take [20]

$$\mathcal{D}(r,t) = \mathcal{D}_{F,0} - \left(\mathcal{D}_{F,0} - \mathcal{D}_F\right)\left[\frac{W(r,t)}{W_0}\right]^{\frac{1}{3}}, \qquad (7)$$

where $\mathcal{D}_{F,0} = 1.5 \times 10^{-6}\mathrm{cm}^2\mathrm{s}^{-1}$ is the diffusion coefficient of F-DNA in water, taken as a typical value; $\mathcal{D}_F = 0.97 \times 10^{-11}\mathrm{cm}^2\mathrm{s}^{-1}$ is the diffusion coefficient of the same molecules inside fully cross-linked alginate; W_0 is the crosslinking density of the intact alginate. The diffusion coefficient of F-DNA in the intact cross-linked gel was also taken from the same as in the earlier work [20]. With these assumptions, the calculated F-DNA leakage curve, Figure 5(a), is a in good agreement with the experimental data.

The diffusion equation for F-DNA, with its initial concentration F_0, in a cylindrical alginate film is

$$\frac{\partial F(r,t)}{\partial t} = \mathcal{D}(r,t)\left[\frac{\partial^2 F(r,t)}{\partial r^2} + \frac{1}{r}\frac{\partial F(r,t)}{\partial r}\right] . \quad (8)$$

The initial concentration of the FAM-labelled DNA in alginate, 0.07 μM, was calculated using the calibration coefficient 1.12×10^{-3} nM (a.u.)$^{-1}$ reported in Section 2.3.5, and the maximum measured signal, Figure 5(b). This initial concentration is approximately 12 times smaller than the concentration of F-DNA in alginate solution during the preparation stage, see Section 2.3.1. The diffusion of all the other mobile species, i.e., A, G, B, Q, L, C, D and H, inside alginate and in solution — which we limited to a thin layer, 0.2 mm, of solution outside the alginate, which is affected by diffusion (without accounting for convection) on time scales tens of minutes — is modelled by using equations similar to Equation (8) with $\mathcal{D}(r,t) = \mathcal{D}_0$.

At any arbitrary time, t, the concentration of the released F-DNA in the cuvette is calculated according to:

$$F_s(t) = \frac{2}{V}\pi Z \int_R^{R+X} r[F_0 - F(r,t)]dr, \quad (9)$$

where $V = 1.5$ mL is the volume of the solution in a cuvette for the measurements. For comparison with the experimental measurements the quantity $F_s(t)$ was converted to the output signal, $S(t)$, using the aforementioned calibration coefficient.

The effective rate constant of the reduction of cross-linking in the hydrogel due to H_2O_2, k_5, was determined by the least square fit together with k_4, the rate constant of oxidation of lactate to pyruvate and also production of hydrogen peroxide, from Figure 5(b). After these two parameters were found, the rate constant of reduction of pyruvate to lactate, k_3, was determined from the next data set, see Figure 5(c). Next, the rate constant of oxidation of glucose to gluconic acid, k_2, was determined from the experiment Figure 5(d). Lastly the rate of conversion of maltose to glucose, k_1, was fitted from the data set Figure 5(e). The values of k_1 and k_2 were not determined precisely due to small value of k_3 which makes it an overall reaction-limiting step. In summary, rate parameter fitting yielded the model curves that agree reasonably well with the

experiment data, see Figure 5, for various combinations of the input and "machinery" chemicals. The fitted values for these rate parameters are

$$
\begin{aligned}
&k_1 = 1.5 \times 10^{-3}\ \mathrm{s}^{-1}\ , \\
&k_2 = 0.4 \times 10^{-3}\ \mathrm{mM}^{-1}\mathrm{s}^{-1}\ , \\
&k_3 = 0.3 \times 10^{-6}\ \mathrm{mM}^{-1}\mathrm{s}^{-1}\ , \\
&k_4 = 0.1 \times 10^{-3}\ \mathrm{mM}^{-1}\mathrm{s}^{-1}\ , \\
&k_5 = 0.1 \times 10^{-3}\ \mathrm{mM}^{-1}\mathrm{s}^{-1}\ .
\end{aligned}
\qquad (10)
$$

In the simulation experiments corresponding to Figure 5(c), (d) and (e), average H_2O_2 concentration inside alginate (and in a 0.2 mm layer of solution) increases approximately linearly to 0.04 mM by 400 min. For the case corresponding to Figure 5(b), H_2O_2 reaches steady-state concentration of approximately 0.3 mM after about 120 min. Note that this is not the bulk concentration in the cuvette but the concentration inside and somewhat outside the alginate layer, and that these hydrogen peroxide levels are low enough not to significantly hinder the enzymes' activity. We also note that among $k_{2,3,4}$, the rate k_3 is a couple of orders of magnate smaller, which confirms the expectation that the LDH-catalyzed step is the bottleneck reaction in this cascade. In fact, this is likely due a certain degree of reversibility known [49] for the action of enzyme LDH, which is not properly accounted for in our modeling, see Equation (3). As a result of the latter, the model does not fit well the short-time data in data sets presented in Figure 5(c), (d), (e).

4. Conclusions

We demonstrated that a complex biocatalytic cascade with many reaction steps can be successfully realized for triggering alginate hydrogel dissolution at the electrode surface and F-DNA release processes, with the biocatalytic reactions taking place at an LBL layer at the surface of the alginate film. The reported approach allowed investigation of a circuit of concatenated logic AND gates and an Identity gate, activated by combinations of four chemical input signals that trigger the F-DNA release, in the framework of recently developed unconventional computing approach based on enzyme-catalyzed reactions. The reaction and

diffusion mechanism of this release system were investigated by means of theoretical modeling. We modelled the key steps in the cascade of enzymatic processes assuming fast diffusion of all the mobile chemicals, and slow diffusion of F-DNA in the hydrogel. The longer biocatalytic cascades that include AMG and GDH (the first two steps in the "network") show the same rate of the process, suggesting the bottleneck reaction step associated with LDH, which was confirmed by modeling.

The present work demonstrated for the first time the multi-step process triggered by complex biomolecular signals and resulting in the release from the polymer-modified electrode surface. The studied approach can be applied to electrode arrays (see Figure SI-1 in the Supporting Information), which are currently under study, where each electrode is responding to different biomolecular signals and their complex combinations. In addition to biomolecular signals, the release process can be activated by electrochemical signals as has been shown previously [22,23]. Overall, the developed approach allows activation of the biomolecular release processes from modified electrodes activated by complex combinations of the electrochemical and biochemical signals.

Acknowledgement

This work was supported by National Science Foundation, USA, (award CBET-1403208) and by Russian Science Foundation (project no. 17-13-01096).

Supporting information for this article is available on the WWW under
http://dx.doi.org/10.1002/elan.....

References

[1] *Controlled Release Systems: Advances in Nanobottles and Active Nanoparticles*, A. van Herk, J. Forcada, G. Pastorin (Eds.), CRC Press, Boca Raton, **2016**.

[2] *Fundamentals and Applications of Controlled Release Drug Delivery*, J. Siepmann, R. A. Siegel, M. J. Rathbone (Eds.), Springer, New York, **2012**.

[3] C. Z. Ding, Z. B. Li, *Mater. Sci Eng. C* **2017**, *76*, 1440–1453.

[4] C. D. Ding, L. Tong, J. Feng, J. J. Fu, *Molecules* **2016**, *21*, art. No. 1715.

[5] N. H. Maniya, S. R. Patel, Z. V. P. Murthy, *Rev. Adv. Mater. Sci.* **2016**, *44*, 257–272.

[6] R. A. Perez, R. K. Singh, T.-H. Kim, H.-W. Kim, *Mater. Horizons* **2017**, *4*, 772–799.

[7] Z.-Q. Cao, G.-J. Wang, *Chem. Record* **2016**, *16*, 1398–1435.

[8] K. Ulbrich, K. Hola, V. Subr, A. Bakandritsos, J. Tucek, R. Zboril, *Chem. Rev.* **2016**, *116*, 5338–5431.

[9] Y. Zhang, S. Sinha-Ray, A. L. Yarin, *J. Mater. Chem.* **2011**, *21*, 8269–8281.

[10] G. Kocak, C. Tuncer, V. Butun, *Polymer Chem.* **2017**, *8*, 144–176.

[11] D. Mertz, O. Sandre, S. Begin-Colin, *Biochim. Biophys. Acta* **2017**, *1861*, 1617–1641.

[12] N. Z. Knezevic, *J. Nanosci. Nanotechnol.* **2016**, *16*, 4195–4199.

[13] S. Szunerits, F. Teodorescu, R. Boukherroub, *Eur. Polym. J.* **2016**, *83*, 467–477.

[14] B. Alshammary, F. C. Walsh, P. Herrasti, C. P. de Leon, J. Solid State Electrochem. 2016, 20, 839–859.

[15] E. Honarvarfard, M. Gamella, N. Guz, E. Katz, *Electroanalysis* **2017**, *29*, 324–329.

[16] *Alginates: Biology and Applications*, Microbiology Monographs Series, B. H. A. Rehm (Ed.), Vol. 13, Springer, Dordrecht, The Netherlands, **2009**.

[17] W. R. Gombotz, S. F. Wee, *Adv. Drug Delivery Rev.* **2012**, *64*, 194–205.

[18] S. Mandal, S. K. Basu, B. Sa, Carbohydrate Polym. **2010**, *82*, 867–873.

[19] A. R. Fajardo, M. B. Silva, L. C. Lopes, J. F. Piai, A. F. Rubira, E. C. Muniz, *RSC Adv.* **2012**, *2*, 11095–11103.

[20] S. Scheja, S. Domanskyi, M. Gamella, K. L. Wormwood, C. C. Darie, A. Poghossian, M. J. Schöning, M. Melman, V. Privman, E. Katz, *ChemPhysChem* **2017**, *18*, 1541–1551.

[21] R. G. Pearson, *J. Am. Chem. Soc.* **1963**, *85*, 3533−3539.

[22] Z. Jin, G. Güven, V. Bocharova, J. Halámek, I. Tokarev, S. Minko, A. Melman, D. Mandler, E. Katz, *ACS Appl. Mater. Interfaces* **2012**, *4*, 466–475.

[23] Z. Jin, A. M. Harvey, S. Mailloux, J. Halámek, V. Bocharova, M. R. Twiss, E. Katz, *J. Mater. Chem.* **2012**, 22, 19523–19528.

[24] M. Gamella, N. Guz, E. Katz, *Electroanalysis* **2016**, *28*, 2692–2696.

[25] M. Gamella Carballo, N. Guz, J. M. Pingarrón, R. Aslebagh, C. C. Darie, E. Katz, *Chem. Commun.* **2015**, *51*, 7618–7621.

[26] E. Katz, J. M. Pingarrón, S. Mailloux, N. Guz, M. Gamella, G. Melman, A. Melman, *J. Phys. Chem. Lett.* **2015**, *6*, 1340–1347.

[27] M. Gamella, N. Guz, S. Mailloux, J. M. Pingarrón, E. Katz, *Electroanalysis* **2014**, *26*, 2552–2557.

[28] M. Gamella, N. Guz, S. Mailloux, J. M. Pingarrón, E. Katz, *ACS Appl. Mater. Interfaces* **2014**, *6*, 13349–13354.

[29] S. Mailloux, N. Guz, A. Zakharchenko, S. Minko, E. Katz, *J. Phys. Chem. B* **2014**, *118*, 6775–6784.

[30] S. Mailloux, N. Guz, M. Gamella Carballo, J. M. Pingarrón, E. Katz, *Anal. Bioanal. Chem.* **2014**, *406*, 4825–4829.

[31] S. Mailloux, J. Halámek, E. Katz, *Analyst* **2014**, *139*, 982–986.

[32] S. Mailloux, J. Halámek, L. Halámková, A. Tokarev, S. Minko, E. Katz, *Chem. Commun.* **2013**, *49*, 4755–4757.

[33] C. S. Kyoung, C. Y. Sung, *Polymer – Korea* **2011**, *35*, 444–450.

[34] H. K. Holme, L. Davidsen, A. Kristiansen, O. Smidsrod, *Carbohydrate Polymers* **2008**, *73*, 656–664.

[35] Z. Yang, J. P. Li, H. S. Guan, *Carbohydrate Polymers* **2004**, *58*, 115–121.

[36] X. X. Li, A. H. Xu, H. G. Xie, W. T. Yu, W. Y. Xie, X. J. Ma, *Carbohydrate Polymers* **2010**, *79*, 660–664.

[37] S. R. Mao, T. T. Zhang, W. Sun, X. H. Ren, *Pharm. Development Technol.* **2012**, *17*, 763–769.

[38] O. Smidsrød, A. Haug, B. Larsen, *Acta Chem. Scand.* **1965**, *19*, 143–152.

[39] S. Goldstein, D. Meyerstein, G. Czapski, *Free Radical Biology and Medicine* **1993**, *15*, 435–445.

[40] M. Gamella, M. Privman, S. Bakshi, A. Melman, E. Katz, *ChemPhysChem* **2017**, *18*, 1811–1821.

[41] *Unconventional Computation. Lecture Notes in Computer Science*, Vol. 5715 (Eds.: C. S. Calude, J. F. Costa, N. Dershowitz, E. Freire, G. Rozenberg), Springer, Berlin, **2009**.

[42] E. Katz, V. Privman, *Chem. Soc. Rev.* **2010**, *39*, 1835–1857.

[43] E. Katz, *Curr. Opin. Biotechnol.* **2015**, *34*, 202–208.

[44] V. Privman, O. Zavalov, L. Halámkova, F. Moseley, J. Halámek, E. Katz, *J. Phys. Chem. B* **2013**, 117, 14928 –14939.

[45] V. Privman, M. A. Arugula, J. Halámek, M. Pita, E. Katz, *J. Phys. Chem. B* **2009**, 113, 5301– 5310.

[46] V. Privman, G. Strack, D. Solenov, M. Pita, E. Katz, *J. Phys. Chem. B* **2008**, 112, 11777–11784.

[47] G. A. Truesdale, A. L. Downing, *Nature* **1954**, *173*, 1236.

[48] Y. Wu, S. Joseph, N. R. Aluru, *J. Phys. Chem. B* **2009**, *113*, 3512–3520.

[49] R. E. Vanderlinde, *Ann. Clin. Lab. Sci.* **1985**, *15*, 13–31.